The 6th International Conference on Renewable Power Generation (RPG)

19–20 October 2017

Three-phase dynamic phasor model of HVDC systems

Gang Luo[1], Chongru Liu[2], Feng Qian[2], Yinguo Yang[2], Junlei Liu[2], Yunhao Zhao[2], Wei Xu[1]

[1]*Guangdong Power Grid Co. Limited, Guangzhou, People's Republic of China*
[2]*North China Electric Power University, Beijing, People's Republic of China*
E-mail: 1518693584@qq.com

Published in *The Journal of Engineering*; Received on 12th October 2017; Accepted on 2nd November 2017

Abstract: A three-phase dynamic phasor (TPDP) model of high-voltage direct current (HVDC) systems is proposed. The proposed TPDP model of HVDC systems can rapidly solve the dynamic characteristics of HVDC systems under the asymmetrical conditions of an alternating current system. The switch function model of the converter is enhanced according to commutation process analysis of the converter. Due to the frequency characteristics analysis results, the TPDP model of the HVDC systems including the converter, DC line, and controller are established through dynamic phasor theory. Simulation results show that the proposed model is effective and acceptable.

1 Introduction

High voltage direct current (HVDC) transmission technology has been widely used in the world because of its advantage of long-distance large-capacity transmission. Especially in China, 24 HVDC transmission projects have been built until 2017 and the Chinese power grid has been the most complex alternating current (AC)–direct current (DC) interconnected power grid with the most number of HVDC transmission projects in the world [1]. To analyse the dynamic process of the AC–DC system, the difference modelling and simulation methods of HVDC systems having different levels of details and being suitable for different research purposes have been an important research topic.

Nowadays, the simulation models of HVDC transmission systems used in the power system simulation widely are divided into two categories: the electromagnetic transient (EMT) model [2] and the electromechanical transient model [3]. The EMT model can reflect the dynamic process of the fundamental frequency and other harmonics under the symmetrical and asymmetrical conditions of AC systems, but this simulation model needs a lot of computer calculating resources and is unsuitable for simulation of large-scale power systems. The EMT model uses the quasi-steady-state model of power systems where steady-state-equations and root-mean-square values are used and are suitable for large-scale power systems, but it only represents the fundamental frequency response of power systems. To solve the contradiction between simulation precision and simulation scale, the dynamic phasor theory is introduced into the modelling and simulation of power systems [4]. This theory deduces the time-varying Fourier series of the main time-domain signals of power system models based on Fourier transformation to build their dynamic phasor models reflecting the dynamic characteristics of the power system. Simulation models of the converter of power electronic devices which are differential models in the EMT simulation can be built as an algebraic model based on the dynamic phasor theory and dynamic phasor models of dominant frequency components of the converter can be built according to the demand of simulation accuracy. This theory has been widely used in modellings and simulations of HVDC systems under symmetrical conditions of AC systems [4, 5], the converter of HVDC systems under asymmetrical conditions of AC systems [6, 7], grid-connected rectifiers [8–11], modular multi-level converters [12] and some other power electronic devices. However, the switch functions built in [6] do not consider the influence of commutation angle adequately and cannot represent the switch and commutation process accurately, the dynamic phasor models built in [7] only consider the fundamental component in the AC side and DC component in the DC side and cannot fully represent the main frequency characteristic of HVDC systems.

We focus on the three-phase dynamic phasor (TPDP) model of HVDC systems including the models of the converter, DC line, and controller to represent the main frequency characteristics of HVDC systems under asymmetrical conditions of AC systems. The following sections are organised as follows: Section 2 establishes the switch functions model for the converter considering the influence of commutation angle under asymmetrical conditions of AC systems adequately. Section 3 proposes the TPDP model of HVDC systems based on the established switch functions model and the frequency analysis of HVDC systems under the asymmetrical conditions of AC systems. Section 4 analyses the simulation process of the proposed TPDP model. Section 5 shows the simulation results and Section 6 draws the conclusions of this study.

2 Switch function model considering commutation angle

The 6-plus HVDC transmission systems are shown in Fig. 1, where L_r and L_i are commutation reactors for rectifiers and inverters; L_d is the DC line flat wave reactance; R_d is the DC line resistance; C_d is the parasitic capacitance of the DC line to ground; v_{dr} and i_{dr} are the voltage and current at the DC side of the rectifier, respectively, v_{di} and i_{di} are voltage and current at the DC side of the inverter, respectively; v_{dc} and i_{dc} are voltage and current of the DC capacitor, respectively; v_{ra}, v_{rb}, v_{rc}, i_{ra}, i_{rb} and i_{rc} are the AC side voltage and current of the rectifier, respectively; v_{ia}, v_{ib}, v_{ic}, i_{ia}, $i_{ib,}$ and i_{ic} are the AC side voltage and current of the inverter, respectively.

The waveform of the switch function shown in Fig. 2 considers the offset effect of the commutation angle and can reflect the switch and commutation process of the converter accurately, where α and μ are firing angle and commutation angle, respectively, its Fourier series expression is shown as

$$S = \sum_{n=1}^{\infty} A_n \cos\left(\frac{n\mu}{2}\right) \cos n\left(\omega t - \alpha - \frac{\mu}{2}\right), \quad (1)$$

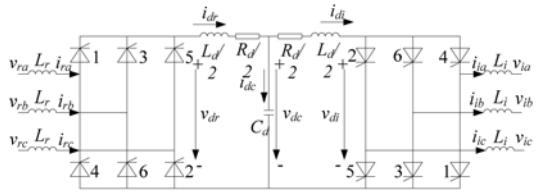

Fig. 1 *Schematic diagram of DC transmission system*

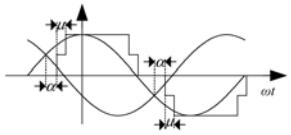

Fig. 2 *Diagram of switch function waveform*

where n is a positive integer, $A_n=(4/\pi n)\sin(\pi n/2)\cos(\pi n/6)$. $A_n=0$ when n is a multiple of 2 or 3.

Suppose the three-phase voltage is shown as follows:

$$\begin{bmatrix} v_a \\ v_b \\ v_c \end{bmatrix} = \begin{bmatrix} v_a \cos(\omega t + \varphi_{va}) \\ v_b \cos\left(wt + \varphi_{vb} - \dfrac{2\pi}{3}\right) \\ v_c \cos\left(wt + \varphi_{vc} - \dfrac{2\pi}{3}\right) \end{bmatrix}, \tag{2}$$

where φ_{va}, φ_{vb}, and φ_{vc} are initial phase angles of the three-phase voltage.

Ignore the error of the commutation phase angle of converter μ caused by φ_{va}, φ_{vb} and φ_{vc}, the commutation angle of the converter can be calculated by using the following equation [6]:

$$\mu = \cos^{-1}\left(\cos\alpha - \frac{\sqrt{2}X_r i_d}{E}\right) - \alpha, \tag{3}$$

where X_r is the leakage reactance of the converter transformer and E is the effective value of the line voltage at the converter side of the converter transformer.

The voltage and current switch functions are shown as follows:

$$\begin{cases} S_{va} = \sum_{n-1}^{\infty} A_n \cos\left(\dfrac{n\mu}{2}\right)\cos n\left(\omega t - \alpha - \dfrac{\mu}{2} + \varphi_{va}\right), \\ S_{vb} = \sum_{n-1}^{\infty} A_n \cos\left(\dfrac{n\mu}{2}\right)\cos n\left(\omega t - \alpha - \dfrac{\mu}{2} + \varphi_{vb} - \dfrac{2\pi}{3}\right), \\ S_{vc} = \sum_{n-1}^{\infty} A_n \cos\left(\dfrac{n\mu}{2}\right)\cos n\left(\omega t - \alpha - \dfrac{\mu}{2} + \varphi_{vc} - \dfrac{2\pi}{3}\right), \end{cases} \tag{4}$$

$$\begin{cases} S_{ia} = \sum_{n-1}^{\infty} A_n \dfrac{\sin(n\mu/2)}{n\mu}\cos n\left(\omega t - \alpha - \dfrac{\mu}{2} + \varphi_{va}\right), \\ S_{ib} = \sum_{n-1}^{\infty} A_n \dfrac{\sin(n\mu/2)}{n\mu}\cos n\left(\omega t - \alpha - \dfrac{\mu}{2} + \varphi_{vb} - \dfrac{2\pi}{3}\right), \\ S_{ic} = \sum_{n-1}^{\infty} A_n \dfrac{\sin(n\mu/2)}{n\mu}\cos n\left(\omega t - \alpha - \dfrac{\mu}{2} + \varphi_{vc} - \dfrac{2\pi}{3}\right). \end{cases} \tag{5}$$

3 TPDP model of HVDC systems

The TPDP model of HVDC systems includes the TPDP model of the rectifier and inverter of HVDC systems, the TPDP model of the DC circuit, and the dynamic phasor model of the controller. Detailed models are given below.

3.1 TPDP model of the converter

When asymmetric faults happen at AC systems, the main non-characteristic harmonics reflecting the dynamic characteristics of AC–DC systems are that the DC voltage and DC current at the DC side contain DC and second harmonic components and the AC current at the AC side of the converter contains the fundamental and third harmonic components [6]. According to the switch function model, the modulation theory of the converter [13] and the dynamic phasor theory [6], assume that the fundamental frequency of the power system is f_0, and the AC system has asymmetric faults, the dynamic phasor model of the DC voltage of the TPDP model of the rectifier as

$$\begin{aligned} \langle v_{dr}\rangle_0(t) &= \frac{1}{2}(V_{ra}(t) + V_{rb}(t) \\ &\quad + V_{rc}(t))A_1 \cos\frac{\mu_r(t)}{2}\cos\left(\alpha_r(t) + \frac{\mu_r(t)}{2}\right) \\ \langle v_{dr}\rangle_2(t) &= \frac{A_1}{4}\cos\frac{\mu_r(t)}{2}\left(V_{ra}(t)e^{j(-\alpha_r(t)-(\mu_r(t)/2)+2\varphi_{vra})}\right. \\ &\quad + V_{rb}(t)e^{j(-\alpha_r(t)-(\mu_r(t)/2)+2\varphi_{vrb}-(4\pi/3))} \\ &\quad \left. + V_{rc}(t)e^{j(-\alpha_r(t)-(\mu_r(t)/2)+2\varphi_{vrc}+(4\pi/3))}\right). \end{aligned} \tag{6}$$

The dynamic phasor model of the AC current at the AC side of the TPDP model of the rectifier as

$$\begin{bmatrix} \langle i_{ra}\rangle_1(t) \\ \langle i_{rb}\rangle_1(t) \\ \langle i_{rc}\rangle_1(t) \end{bmatrix} = \begin{bmatrix} \langle i_{dr}S_{ira}\rangle_1(t) \\ \langle i_{dr}S_{irb}\rangle_1(t) \\ \langle i_{dr}S_{irc}\rangle_1(t) \end{bmatrix} = \begin{bmatrix} \langle i_{dr}\rangle_0(t)\langle S_{ira}\rangle_1(t) + \langle i_{dr}\rangle_2(t)\langle S_{ira}\rangle_1^*(t) \\ \langle i_{dr}\rangle_0(t)\langle S_{irb}\rangle_1(t) + \langle i_{dr}\rangle_2(t)\langle S_{irb}\rangle_1^*(t) \\ \langle i_{dr}\rangle_0(t)\langle S_{irc}\rangle_1(t) + \langle i_{dr}\rangle_2(t)\langle S_{irc}\rangle_1^*(t) \end{bmatrix},$$
$$\begin{bmatrix} \langle i_{ra}\rangle_3(t) \\ \langle i_{rb}\rangle_3(t) \\ \langle i_{rc}\rangle_3(t) \end{bmatrix} = \begin{bmatrix} \langle i_{dr}S_{ira}\rangle_3(t) \\ \langle i_{dr}S_{irb}\rangle_3(t) \\ \langle i_{dr}S_{irc}\rangle_3(t) \end{bmatrix} = \begin{bmatrix} \langle i_{dr}\rangle_2(t)\langle S_{ira}\rangle_1(t) + \langle i_{dr}\rangle_2^*(t)\langle S_{ira}\rangle_5(t) \\ \langle i_{dr}\rangle_2(t)\langle S_{irb}\rangle_1(t) + \langle i_{dr}\rangle_2^*(t)\langle S_{irb}\rangle_5(t) \\ \langle i_{dr}\rangle_2(t)\langle S_{irc}\rangle_1(t) + \langle i_{dr}\rangle_2^*(t)\langle S_{irc}\rangle_5(t) \end{bmatrix}, \tag{7}$$

where

$$\begin{aligned} \langle S_{ira}\rangle_n(t) &= \frac{A_n}{n\mu_r(t)}\sin\frac{n\mu_r(t)}{2}e^{jn(-\alpha_r(t)-(\mu_r(t)/2)+\varphi_{vra})}, \\ \langle S_{irb}\rangle_n(t) &= \frac{A_n}{n\mu_r(t)}\sin\frac{n\mu_r(t)}{2}e^{jn(-\alpha_r(t)-(\mu_r(t)/2)+\varphi_{vrb}-(2\pi/3))}, \\ \langle S_{ira}\rangle_n(t) &= \frac{A_n}{n\mu_r(t)}\sin\frac{n\mu_r(t)}{2}e^{jn(-\alpha_r(t)-(\mu_r(t)/2)+\varphi_{vrc}+(2\pi/3))}. \end{aligned} \tag{8}$$

The TPDP model of the inverter is similar to the TPDP model of the rectifier.

3.2 TPDP model of the DC line

The dynamic equation of the DC line of the HVDC system shown in Fig. 1 as

$$\begin{aligned} \frac{L_d}{2}\frac{di_{dr}}{dt} &= v_{dr} - v_{dc} - \frac{R_d}{2}i_{dr}, \\ \frac{L_d}{2}\frac{di_{di}}{dt} &= v_{dc} - v_{di} - \frac{R_d}{2}i_{di}, \\ C_{dc}\frac{dv_{dc}}{dt} &= i_{dc}. \end{aligned} \tag{9}$$

According to the frequency characteristics of the DC side of HVDC

doi: 10.1049/joe.2017.0731

systems [6], the TPDP model of the DC line as

$$\begin{cases} \dfrac{L_d}{2}\dfrac{d\langle i_{dr}\rangle_0}{dt} = \langle v_{dr}\rangle_0 - \langle v_{dc}\rangle_0 - \dfrac{R_d}{2}\langle i_{dr}\rangle_0, \\ \dfrac{L_d}{2}\dfrac{d\langle i_{di}\rangle_0}{dt} = \langle v_{dc}\rangle_0 - \langle v_{di}\rangle_0 - \dfrac{R_d}{2}\langle i_{di}\rangle_0, \\ C_{dc}\dfrac{d\langle v_{dc}\rangle_0}{dt} = \langle i_{dc}\rangle_0, \end{cases} \tag{10}$$

$$\begin{cases} \dfrac{L_d}{2}\dfrac{d\langle i_{dr}\rangle_2}{dt} = \langle v_{dr}\rangle_2 - \langle v_{dc}\rangle_2 - \dfrac{R_d}{2}\langle i_{dr}\rangle_2 - j\omega L_d\langle i_{dr}\rangle_2, \\ \dfrac{L_d}{2}\dfrac{d\langle i_{di}\rangle_2}{dt} = \langle v_{di}\rangle_2 - \langle v_{dc}\rangle_2 - \dfrac{R_d}{2}\langle i_{di}\rangle_2 - j\omega L_d\langle i_{di}\rangle_2, \\ C_{dc}\dfrac{d\langle v_{dc}\rangle_2}{dt} = \langle i_{dc}\rangle_2 - j2\omega C_{dc}\langle v_{dc}\rangle_2. \end{cases}$$

3.3 Dynamic phasor model of the controller

The constant current control and constant extinction angle control are usually used at the rectifier and inverter of HVDC systems, respectively, and current error control and voltage dependent current control are also used [14].

The structure of the constant current control used at the rectifier is shown in Fig. 3, where K_r and T_r are the proportional constant and integral time constant of proportional-integral controller, respectively. i_{dr} is a measured value of the DC line current at the rectifier side, i_{drref} is a reference value of the DC current, β_r and α_r are advanced firing and firing angles of the rectifier, respectively.

The dynamic equation of the constant current control is as follows:

$$\begin{aligned} &\frac{dx_r}{dt} = -\frac{1}{T_r}i_{dr} + \frac{1}{T_r}i_{drref}, \\ &\alpha_r(t) = \pi - x_r(t) - K_r(i_{drref}(t) - i_{dr}(t)). \end{aligned} \tag{11}$$

Considering the filtering action of the measurement system in the actual system, the controller considers the 0-order dynamic phasor. The dynamic phasor model of the constant current control is as follows:

$$\begin{aligned} &\frac{d\langle x_r\rangle_0}{dt} = -\frac{1}{T_r}\langle i_{dr}\rangle_0 + \frac{1}{T_r}i_{drref}, \\ &\alpha_r = \pi - \langle x_r\rangle_0 - K_r\left(i_{drref} - \langle i_{dr}\rangle_0\right). \end{aligned} \tag{12}$$

The structure of constant current control used at the inverter is similar to the constant current control used at the rectifier. To maintain the stability of the controller, the reference value of the DC current of the constant current control used at the inverter is lower than that at the rectifier by 10%.

When the constant extinction angle control and current error control are used at the inverter, the DC voltage of the inverter is as follows:

$$v_{di} = v_{di0}cos(\gamma_{ref} + \gamma_{err}) - \frac{3}{\pi}\omega L_i i_{di}, \tag{13}$$

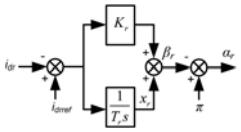

Fig. 3 *Structure diagram of the rectifier current controller*

where γ_{ref} is the reference value of the extinction angle of the constant extinction angle control and γ_{err} is the increment of the extinction angle outputted by the current error control. The DC voltage of the inverter can also be calculated using (14) by the advanced firing angle β_i

$$v_{di} = v_{di0}cos\beta_i + \frac{3}{\pi}\omega L_i i_{di}. \tag{14}$$

Consider (13) and (14), we can obtain the control law of the constant extinction angle control used at the inverter as

$$\begin{aligned} &\beta_i(t) = \arccos\left(\cos(\gamma_{ref} + \gamma_{err}(t)) - \frac{6}{\pi v_{di0}(t)}\omega L_i i_{di}(t)\right), \\ &\alpha_i(t) = \pi - \beta_i(t). \end{aligned} \tag{15}$$

Therefore, the dynamic phasor model of the constant extinction angle control used at the inverter as

$$\begin{aligned} &\beta_i = \arccos\left(\cos(\gamma_{ref} + \gamma_{err}) - \frac{6}{\pi\langle v_{di0}\rangle_0}\omega L_i\langle i_{di}\rangle_0\right), \\ &\alpha_i = \pi - \beta_i. \end{aligned} \tag{16}$$

The coordination among the controllers is described in [15].

4 Simulation process of three phase dynamic phasor model

To obtain the input of the model easily, the input is the time domain values of the three-phase voltage of AC systems, and the output is the time domain values of the DC voltage, the DC current, and the AC current. The simulation process of the proposed model is achieved by the dynamic phasor. Therefore, the conversion between dynamic phasor values and time domain values is required.

According to the definition of the dynamic phasor, when the simulation step is Δt, the transformation from the time domain values to the values of the kth order dynamic phase as

$$\begin{aligned} \langle X\rangle_k(t) &= \frac{1}{T}\int_{t-T}^{t} x(\tau)e^{-jk((2\pi)/T)\tau}d\tau \\ &= \frac{1}{N}\sum_{n=0}^{N-1} x(t - T + n\Delta t)e^{-jk((2\pi)/T)(t-T+n\Delta t)}, \end{aligned} \tag{17}$$

where $N = T/\Delta t$.

The transformation from the dynamic phasor values of the DC voltage, v_d, the DC current, i_d and the AC current, i_{ra}, i_{rb}, i_{rc}, to time domain values as

$$\begin{aligned} v_d(t) &= \langle v_d\rangle_0(t) + \langle v_d\rangle_2(t)e^{j2\omega t} + \langle v_d\rangle_{-2}(t)e^{-j2\omega t} \\ &= \langle v_d\rangle_0(t) + 2\mathrm{Re}\left(\langle v_d\rangle_2(t)e^{j2\omega t}\right), \end{aligned} \tag{18}$$

$$\begin{aligned} i_d(t) &= \langle i_d\rangle_0(t) + \langle i_d\rangle_2(t)e^{j2\omega t} + \langle i_d\rangle_{-2}(t)e^{-j2\omega t} \\ &= \langle i_d\rangle_0(t) + 2\mathrm{Re}\left(\langle i_d\rangle_2(t)e^{j2\omega t}\right), \end{aligned} \tag{19}$$

(see (20))

The simulation method of the proposed TPDP model is: use the implicit trapezoidal integration method to difference dynamic phasor models of the DC line and the controller, then the processed dynamic phasor models of the DC line and the controller combine with dynamic phasor models of the rectifier and the inverter to achieve the simulation. The simulation process of the TPDP model proposed in this study is shown in Fig. 4, the model of the controller delay models of the converter and the DC line one simulation step.

doi: 10.1049/joe.2017.0731

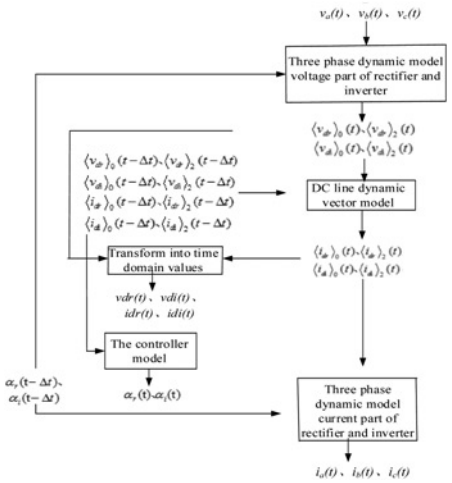

Fig. 4 *Simulation process of TPDP model of HVDC systems*

5 Simulation analysis

5.1 Simulation test system

The simulation test system is the 12-pluse monopolar HVDC system shown in Fig. 5. The effective values of line voltages of AC systems at the rectifier and inverter side are 345 and 230kV, respectively, the converter transformer ratio from AC side to converter side at the rectifier side is 345/213.4557, the converter transformer ratio form the AC side to converter side at the inverter side is 230/209.2288. The fundamental frequency is 50 Hz. The DC voltage and current are 500 kV and 2 kA, respectively. The resistance and inductance of the DC line are 5 Ω and 1.19 H, respectively, the capacitance is 50 μF.

The constant current control and constant extinction angle control are used at the rectifier side and inverter side, respectively, and the current error control and voltage dependent current control are used. The EMT model of the test HVDC systems is established in the EMT simulation program PSCAD/EMTDC, and simulations of the proposed TPDP model and the TPDP model combined the TPDP model of the converter proposed in [6] with the dynamic phasor model of the DC line and the controller are established by MATLAB codes, where the simulation steps of the EMT model and the dynamic phasor model are 100 and 50 μs, respectively.

5.2 Simulation results

The comparisons among simulation results of the EMT model and dynamic phasor models under the three fault types shown in Table 1 are made. The fault happened at the inverter side consider the type of fault that does not cause the commutation failure and is one kind of ground fault through resistance happened on the AC side of the inverter.

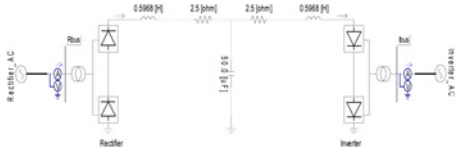

Fig. 5 *Monopolar 12-pulse HVDC systems*

Table 1 Fault types of simulation

Cases	Fault description
fault 1	phase A of the AC side of rectifier is grounded at 1.5 s and lasts 0.05 s
fault 2	phase A of the AC side of rectifier is grounded at 1.5 s and lasts 0.1 s, and phase B is grounded at 1.54 s and last 0.05 s
fault 3	phase A of the AC side of inverter is grounded through resistance R_g at 0.1 s and last 0.1 s, where $R_g = 450\ \Omega$

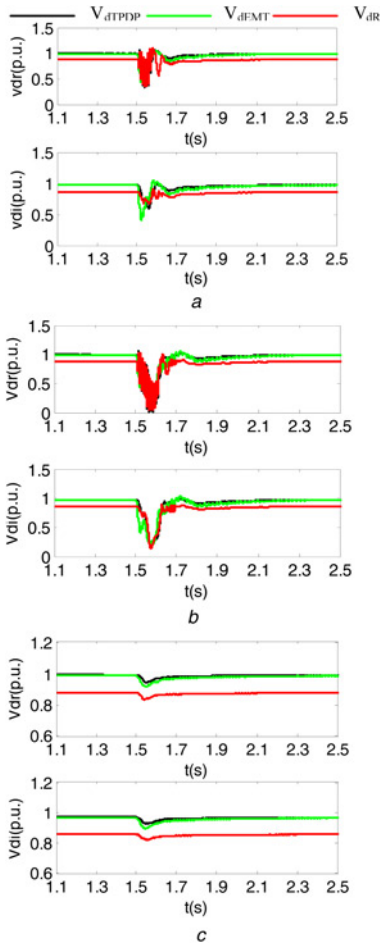

Fig. 6 *Comparisons of DC voltage simulation results*
a Fault 1
b Fault 2
c Fault 3

The simulation results of DC voltages, DC currents and AC currents at the inverter side of TPDP models and the EMT model of HVDC systems under the three asymmetrical faults are shown in Figs. 6–8, respectively, where V_{dTPDP} and I_{dTPDP} are the DC voltage and DC current of the proposed TPDP model of HVDC systems; V_{dR} and I_{dR} are the DC voltage and DC current of the TPDP model proposed in [6]; V_{dEMT} and I_{dEMT} are the DC voltage and DC current of the EMT model of HVDC systems. I_{aTDDP} and I_{aEMT} are the AC currents of Phase A of the AC

$$\begin{bmatrix} i_a(t) \\ i_b(t) \\ i_c(t) \end{bmatrix} = \begin{bmatrix} \langle i_a\rangle_1(t) \\ \langle i_b\rangle_1(t) \\ \langle i_c\rangle_1(t) \end{bmatrix} e^{j\omega t} + \begin{bmatrix} \langle i_a\rangle_{-1}(t) \\ \langle i_b\rangle_{-1}(t) \\ \langle i_c\rangle_{-1}(t) \end{bmatrix} e^{-j\omega t} + \begin{bmatrix} \langle i_a\rangle_3(t) \\ \langle i_b\rangle_3(t) \\ \langle i_c\rangle_3(t) \end{bmatrix} e^{j3\omega t} + \begin{bmatrix} \langle i_a\rangle_{-3}(t) \\ \langle i_b\rangle_{-3}(t) \\ \langle i_c\rangle_{-3}(t) \end{bmatrix} e^{-j3\omega t} = 2\mathrm{Re}\left(\begin{bmatrix} \langle i_a\rangle_1(t) \\ \langle i_b\rangle_1(t) \\ \langle i_c\rangle_1(t) \end{bmatrix} e^{j\omega t} + \begin{bmatrix} \langle i_a\rangle_3(t) \\ \langle i_b\rangle_3(t) \\ \langle i_c\rangle_3(t) \end{bmatrix} e^{j3\omega t} \right). \quad (20)$$

doi: 10.1049/joe.2017.0731

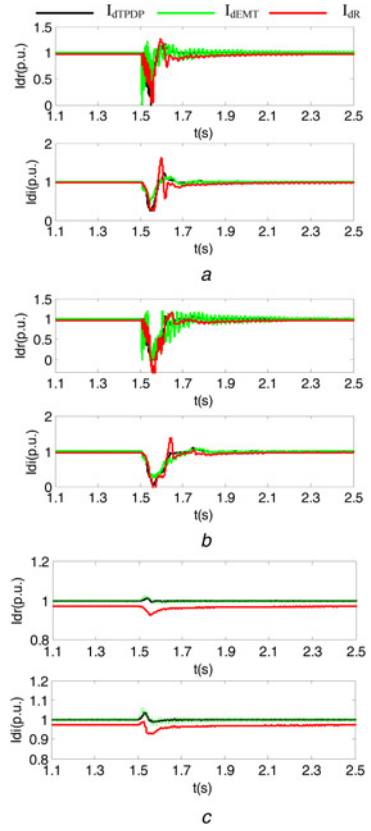

Fig. 7 *Comparison of DC current simulation results*
a Fault 1
b Fault 2
c Fault 3

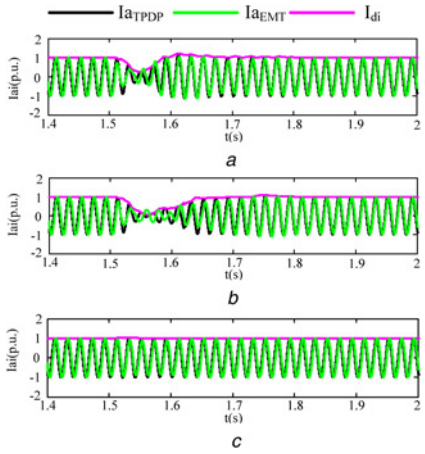

Fig. 8 *Comparison of AC current simulation results*
a Fault 1
b Fault 2
c Fault 3

system at the inverter side of the proposed TPDP model and the EMT model, respectively.

This study only establishes the TPDP model of HVDC systems including the converter, the DC line and the controller under asymmetrical conditions of AC systems, and does not establish the dynamic phasor model of AC filters, reactive power compensation devices, and converter transformers. Use three-phase voltages at the rectifier and inverter side acquired from the EMT model as inputs of TPDP models to verify the effectiveness of the proposed TDPD model. The simulation results shown in Figs. 6 and 7 show that the proposed TPDP model can trace dynamic characteristics of HVDC systems well and is better than the TPDP model proposed in [6]. Since the AC system model has not been established, there are some errors in the AC current at the inverter side.

5.3 *Simulation error analysis*

The residual similarity method is used to analyse the error between the simulation results of the TPDP models and the EMT model. The formula of residual similarity is shown as

$$\gamma_i = \frac{|y_i|}{\sum_{i=1}^{N} |y_i|},$$
$$x_i = 1 - \frac{|y_i - \hat{y}_i|}{\max(|y_i|, |\hat{y}|)}, \tag{21}$$
$$\varphi = \sum_{i=1}^{N} \gamma_i x_i,$$

where y and $\hat{y}$ are simulation results of the EMT model and TPDP model, respectively; x is similarity degree, φ is residual similarity index.

The objects of the residual similarity analysis are time domain values of the DC voltage and the DC current obtained by TPDP models and the EMT model as only the TPDP model of HVDC systems is established. The residual similarities between DC voltages and DC currents of the three faults are shown in Tables 2–4 respectively, where Φ_1 is the residual similarity between the TPDP model proposed and the EMT model, Φ_2 is the residual similarity between the TPDP model proposed in [6] and the EMT model.

When the residual similarity is >80%, the simulation model can meet the requirements of the simulation [15]. The residual similarities between the DC voltage and DC current of the proposed TPDP model are more than 90%, so the proposed model can meet the simulation requirements better.

Table 2 Residual similarity of fault 1

	V_{dr}, %	V_{di}, %	I_{dr}, %	I_{di}, %
Φ_1	95.94	95.81	93.33	96.03
Φ_2	76.60	77.41	75.56	73.24

Table 3 Residual similarity of fault 2

	V_{dr}, %	V_{di}, %	I_{dr}, %	I_{di}, %
Φ_1	93.95	94.35	90.2	94.99
Φ_2	73.89	72.93	74.39	77.29

Table 4 Residual similarity of fault 3

	V_{dr}, %	V_{di}, %	I_{dr}, %	I_{di}, %
Φ_1	98.84	98.82	99.56	99.29
Φ_2	70.61	71.47	69.37	69.48

doi: 10.1049/joe.2017.0731

6 Conclusion

To improve the dynamic model of HVDC systems, this study proposes the TPDP model of HVDC systems by correcting the TPDP model of the converter of HVDC systems used under asymmetrical conditions of AC systems and building the TPDP model of the DC line and dynamic phasor model of the controller, and analyses the simulation process of the proposed TPDP model. The comparisons among the simulation results of the EMT model and TPDP models of HVDC systems show that the proposed TPDP model can use a larger simulation step and dynamic phase model of the converter which is simpler than the EMT model to reflect dynamic characteristics of HVDC systems.

7 Acknowledgements

This work was supported by the project of Power Dispatch Control Centre of Guangdong Power Grid Corp. Ltd (K-GD2014-198): 'Control and Self-Healing Restoration of AC-DC Hybrid Power Systems (Self-Healing Restoration)'.

8 References

[1] Yao L., Jing W.U., Wang Z., *ET AL.*: 'Pattern analysis of future HVDC grid development', *Proc. CSEE*, 2014, **34**, (34), pp. 6007–6020

[2] Liang Y., Lin X., Gole A.M., *ET AL.*: 'Improved coherency-based wide-band equivalents for real-time digital simulators', *IEEE Tran. Power Syst.*, 2011, **26**, (3), pp. 1410–1417

[3] Song X.L., Wu X.C., Liu W.Z., *ET AL.*: 'New quasi-steady-state HVDC models for PSD-BPA power system transient stability simulation program', *Power Syst. Technol.*, 2010, **34**, (1), pp. 62–67

[4] Qi Q., Jiao L., Yan Z., *ET AL.*: 'Modeing and simulation of HVDC systems with dynamic phasors', *Proc. CSEE*, 2003, **23**, (12), pp. 28–32

[5] Zhu H., Cai Z., Liu H., *ET AL.*: 'Hybrid-model transient stability simulation using dynamic phasors based HVDC system model', *Electr. Power Syst. Res.*, 2006, **76**, (6–7), pp. 582–591

[6] Liu C., Bose A., Tian P.: 'Modeling and analysis of HVDC converter by three-phase dynamic phasor', *IEEE Trans. Power Deliv.*, 2014, **29**, (1), pp. 3–12

[7] Wang G., Li Z., Li H., *ET AL.*: 'Dynamic phasor model of the converter of the AC/DC system', *Proc. CSEE*, 2010, **30**, (1), pp. 59–64

[8] Zeng Z., Zhao R., Yang H.: 'Dynamic phasors model of micro-grid with grid-connected inverters and simulation', *Proc. CSEE*, 2012, **32**, (10), pp. 65–71

[9] Wei H., Sun J., Zha X., *ET AL.*: 'Modeling and simulation of microgrid including inverter-interfaced distributed resources based on dynamic phasors', *Autom. Electr. Power Syst.*, 2014, **38**, (3), pp. 686–690

[10] Gu H., An S., Zhao W., *ET AL.*: 'Modeling and simulation of single phase inverter with dynamic phasors', *Adv. Mater. Res.*, 2011, **354–355**, pp. 1381–1385

[11] Nagarajan A., Ayyanar R.: 'Dynamic phasor model of single-phase inverters for analysis and simulation of large power distribution systems'. IEEE Int. Symp. on Power Electronics for Distributed Generation Systems, 2013, pp. 1–6

[12] Deore S.R., Darji P.B., Kulkarni A.M.: 'Dynamic phasor modeling of modular multi-level converters'. IEEE Int. Conf. on Industrial and Information Systems, 2012, pp. 1–6

[13] Hu L., Yacamini R.: 'Harmonic transfer through converters and HVDC links', *IEEE Trans. Power Electron.*, 1992, **7**, (3), pp. 514–525

[14] Xu D., Han M., Ding H., *ET AL.*: 'Modeling of HVDC based on the user-defined model of PSASP', *Autom. Electr. Power Syst.*, 2007, **31**, (6), pp. 71–76

[15] Jia X., Li G., Zhao C.Y., *ET AL.*: 'Study of the credibility evaluation method for the power system simulation', *Proc. CSEE*, 2010, **30**, (19), pp. 51–57